# Boomerang mechanism explaining the excess radio background

P. S. Bhupal Dev,[1,*] Pasquale Di Bari,[2,†] Ivan Martinez-Soler,[3,‡] and Rishav Roshan[4,§]

[1]*Department of Physics and McDonnell Center for the Space Sciences, Washington University, St. Louis, Missouri 63130, USA*

[2]*School of Physics and Astronomy, University of Southampton, Southampton, SO17 1BJ, U.K.*

[3]*Institute for Particle Physics Phenomenology, Department of Physics, Durham University, Durham DH1 3LE, UK*

[4]*School of Physics and Astronomy, University of Southampton, Southampton, SO17 1BJ, UK*

(Dated: October 14, 2025)

We propose a *boomerang mechanism* for the explanation of the excess radio background detected by ARCADE 2. In an early stage of the Universe, at a temperature $T$ in the range $\sim 0.1\,\mathrm{keV}$–$1\,\mathrm{MeV}$, a fraction of relic neutrinos is resonantly converted into dark neutrinos by mixing induced by a pre-existing lepton asymmetry. Dark neutrinos decay much later into a dark-standard photon state and a dark fermion, with a lifetime longer than the age of the Universe, as required by a solution to the excess radio background. This scenario circumvents the upper bound on the neutrino magnetic moment but still implies a testable lower bound.

arXiv:2509.03441v2 [hep-ph] 12 Oct 2025

**Introduction**. The Absolute Radiometer for Cosmology, Astrophysics and Diffuse Emission (ARCADE 2) [1] has detected an excess radio background (ERB) in the 3–10 GHz frequency range with respect to the Cosmic Microwave Background (CMB) thermal spectrum. The excess is statistically significant (more than $5\sigma$) and cannot be explained by known population of sources since they give a contribution to the effective temperature that is 3–10 times smaller than the measured one [2]. Moreover, different observations place a strong upper limit on the anisotropy of the ERB that is, therefore, extremely smooth [3]. This represents a strong constraint for an astrophysical origin and, therefore, the ERB is currently regarded as a mystery [2]. The Tenerife Microwave Spectrometer (TMS) will soon take data in the 10–20 GHz frequency range [4, 5] and might, therefore, help to shed light on this mystery. It was noticed that radiative relic neutrino decay can potentially explain the ARCADE 2 excess [6]. Recently, we have shown that such a solution indeed fits very well the six ARCADE 2 data points between 3–10 GHz giving rise to an excess [7]. It predicts an effective (radiometric) temperature for the non-thermal photons produced by the decays of one of the relic neutrino species, the lightest for definiteness, given by

$$T_{\gamma_{\rm nth}}(E,0) \simeq \frac{6\,\zeta(3)}{11\,\sqrt{\Omega_{\rm M0}}}\,\frac{T_0^3}{E^{1/2}\,\Delta m_1^{3/2}}\,\frac{t_0}{\tau_1}\,\left(1+\frac{a_{\rm D}^3}{a_{\rm eq}^3}\right)^{-\frac{1}{2}}, \tag{1}$$

where $t_0 = 4.35\times 10^{17}\,\mathrm{s}$ is the age of the Universe, $T_0 = (2.725\pm 0.001)\mathrm{K}$ is the photon temperature at the present time measured by the Far Infrared Absolute Spectrophotometer (FIRAS) instrument [8], $\Delta m_1 \equiv m_1 - m_0 \ll m_1$ is the mass difference between the lightest active neutrino and the new sterile state, $\tau_1$ is the neutrino lifetime, $E \leq \Delta m_1$ is the energy of the photon at the present time. For the definition and values of the other cosmological parameters in Eq. (1), see Ref. [7]. This expression can be used to fit the six data points measured by ARCADE 2 in the 3–10 GHz frequency range. The best fit is obtained

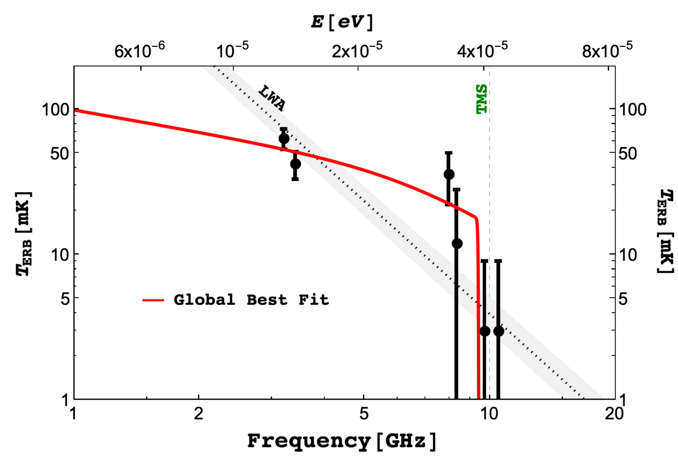


FIG. 1. Best fit curve for $T_{\rm ERB}$ obtained with Eq. (1). The thick red curve corresponds to the best global fit obtained for $\Delta m_1 = 4.0\times 10^{-5}\,\mathrm{eV}$ and $\tau_1 = 1.46\times 10^{21}\,\mathrm{s}$. The ARCADE 2 data points are taken from Ref. [1]. We also show the power-law fit $\beta = -2.58\pm 0.05$ (dotted line with grey shade), obtained using the Long Wavelength Array (LWA) data at lower frequencies [9]. The vertical dashed line shows the TMS low-frequency threshold.

for $\Delta m_1 \simeq 4.0\times 10^{-5}\,\mathrm{eV}$ and $\tau_1 \simeq 1.46\times 10^{21}\,\mathrm{s}$. As shown in Fig. 1, it provides an excellent fit to the ERB temperature spectrum, improving a simple power-law fit, with $\chi^2/\mathrm{d.o.f.} \simeq 1$ with 4 degrees of freedom (d.o.f.) [7]. The result of the fit, expressed in terms of the quantity $\Delta m_1^{3/2}\tau_1$, gives at 99% confidence level (C.L.):

$$(\Delta m_1^{3/2}\tau_1)^{\rm ARCADE} = 3.8^{+7.2}_{-1.5}\times 10^{14}\,\mathrm{eV}^{3/2}\,\mathrm{s}\,. \tag{2}$$

This region is shown in Fig. 2 (shaded regions with different shades for different frequency bands) in the plane $\Delta m_1$ vs. $\tau_1$.

In a general way, we can write the radiative decay rate of the neutrino mass eigenstate $\nu_1$ with mass $m_1$ into another neutrino mass eigenstate $\nu_0$ with mass $m_0$ in

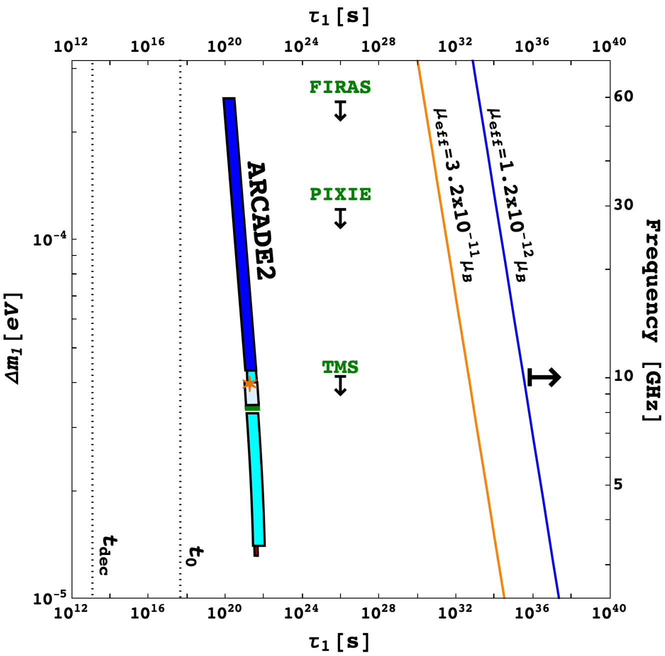


FIG. 2. Allowed region shaded with different shades corresponding to different photon energy bands and with the best-fit point ⋆) explaining the ARCADE 2 excess radio background in the plane of $\Delta m_1$ vs. $\tau_1$ [7]. Lower bounds on the lifetime derived from the upper bound on the effective magnetic transition dipole moment [cf. Eq. (3)] are shown by the blue and orange lines. We also indicate the matter-radiation decoupling time $t_{\rm dec}$ and the current age of the Universe $t_0$. The lowest frequency thresholds for FIRAS, PIXIE and TMS are also indicated.

terms of the *effective magnetic transition dipole moment* $\mu_{\rm eff}$, as [10]

$$\Gamma_{\nu_1\to\nu_0+\gamma} = \frac{(m_1^2-m_0^2)^3}{8\pi\, m_1^3}\,\mu_{\rm eff}^2 \simeq \frac{\Delta m_1^3}{\pi}\,\mu_{\rm eff}^2 \simeq 42.5\,{\rm s}^{-1}\left(\frac{m_1-m_0}{\rm eV}\right)^3\left(\frac{\mu_{\rm eff}}{\mu_{\rm B}}\right)^2 . \tag{3}$$

In the second expression we used $m_1+m_0\simeq 2\,m_1$, since we are interested in the case of quasi-degenerate neutrinos. In the numerical expression we normalised $\mu_{\rm eff}$ to the Bohr magneton $\mu_{\rm B}=e\hbar/(2m_e)\simeq 296.3\,{\rm GeV}^{-1}$. The effective magnetic transition dipole moment is defined as

$$\mu_{\rm eff}\equiv\sqrt{|\mu_{1\to 0}|^2+|\epsilon_{1\to 0}|^2}\,, \tag{4}$$

where $\mu_{1\to 0}$ is the transition magnetic dipole and $\epsilon_{1\to 0}$ is the transition electric dipole moment [11]. The most stringent upper bound on $\mu_{\rm eff}$ comes from plasmon decays in globular cluster stars [12, 13]:

$$\mu_{\rm eff}\lesssim 1.2\times 10^{-12}\,\mu_{\rm B}. \tag{5}$$

In this case, from Eq. (3), one easily finds the following lower bound on the lifetime of $\nu_1$:

$$\tau_{\nu_1\to\nu_0+\gamma}\gtrsim 2.5\times 10^{21}\,{\rm s}\left(\frac{\rm eV}{\Delta m_1}\right)^3 . \tag{6}$$

One can see that for $\Delta m_1\lesssim 10^{-4}\,$eV, a necessary condition to address the ERB, one obtains $\tau_{\nu_1\to\nu_0+\gamma}\gtrsim 10^{33}\,$s, an incredibly long lifetime yielding completely negligible contribution to the ERB. This conclusion remains valid even considering the less stringent laboratory upper bound from the GEMMA experiment measuring electron recoils induced by neutrino-electron elastic scattering [14, 15],

$$\mu_{\rm eff}\lesssim 2.9\times 10^{-11}\,\mu_{\rm B}\,. \tag{7}$$

The situation is depicted in Fig. 2. Therefore, irrespectively of whether the final neutrino is an active or a sterile neutrino species, neutrino radiative decay by itself cannot give any sizable contribution to the ERB.

The *boomerang mechanism* that we propose here provides a way to circumvent this bound, preserving at the same time the success of Eq. (1) in reproducing the ARCADE 2 data. While in radiative neutrino decays ordinary neutrinos directly decay into photons, in the boomerang mechanism neutrinos are first converted into dark (sterile) neutrinos and then these decay into dark photons and standard photons, with the latter constituting the ERB [16]. We first discuss how active-dark neutrino mixing, in the presence of a sufficiently large lepton asymmetry, can convert a fraction of relic neutrinos into (quasi-degenerate) dark neutrinos. Second, we discuss how the dark neutrinos decay into a dark fermion species and into dark and standard photon state. Third, we combine together all constraints and determine an allowed region in the plane of active-dark neutrino mixing angle versus mass squared difference that maps into a corresponding region in the plane of the neutrino effective magnetic moment and resonance temperature. Finally, we draw some final remarks.

**Active-to-dark neutrino conversions in the early Universe**. We assume the existence of a light sterile dark neutrino field almost coinciding with mass eigenstate $\nu_0$ with mass $m_0$ and quasi-degenerate with the lightest neutrino with positive $\Delta m^2\equiv m_1^2-m_0^2$ [17]. We also assume, for definiteness, that it just mixes with the muon neutrino but all results are valid in general. The much higher values of $m_{2,3}^2-m_0^2$ make in a way that the relevant mixing parameters are just $\Delta m^2$ and a very small muon-dark neutrino mixing angle $\theta_0$. With these assumptions and definitions the mixing in the early Universe is described by the effective Hamiltonian $\Delta H$ that in the interaction basis can be written as

$$\Delta H_{\mu-{\rm dark}} = \frac{\Delta m^2}{4\,p}\begin{pmatrix}\cos 2\theta_0 - v(y,T_\nu,L) & -\sin 2\theta_0\\ -\sin 2\theta_0 & -(\cos 2\theta_0 - v(y,T_\nu,L))\end{pmatrix}, \tag{8}$$

where we introduced the dimensionless effective potential

$$v(y,T,L) = v_1(y,T_\nu) + v_2(y,T_\nu,L)\,. \tag{9}$$

In this expression we denoted by $T_\nu$ the neutrino temperature, $y \equiv p/T_\nu$ and by $L$ the effective (muonic) total asymmetry defined as

$$L \equiv 2L_{\nu_\mu} + L_{\nu_e} + L_{\nu_\tau} - \frac{1}{2}B_n\,, \tag{10}$$

where the neutrino asymmetries $L_{\nu_\alpha} \equiv (N_{\nu_\alpha} - N_{\bar\nu_\alpha})/N_\gamma^{\rm i}$ and similarly for the neutron asymmetry $B_n$, with $N_\gamma^{\rm i}$ the photon abundance at some initial time $t_{\rm i}$ such that $m_\mu \gg T_{\rm i} \gg m_e$, with $T_{\rm i} \equiv T(t_{\rm i})$. The term $v_1(y,T_\nu)$ is the finite temperature contribution [18] and is given by

$$v_1(y,T_\nu) = \frac{{\rm eV}^2}{\Delta m^2}\left(\frac{T_\nu}{T_\alpha}\right)^6 y^2\,, \tag{11}$$

where $T_\mu \simeq 23.4$ MeV. For $L=0$ and $\Delta m^2 > 0$, there would be a resonance, both for neutrinos and antineutrinos, at $T_\nu^{\rm res}(y,0) \simeq T_\alpha\,(y^2\,\Delta m^2/{\rm eV}^2)^{1/6}$. At this resonance relic neutrinos are not efficiently converted into dark neutrinos, though this could be used to trigger the generation of a large lepton asymmetry [19, 20], as we comment in the final remarks. However, here we assume that there already exists an initial pre-existing effective muon asymmetry $L_{\rm i}$. In this case one has also to consider the term $v_2(y,T_\nu,L)$ given by [21]

$$v_2(y,T_\nu,L) \simeq \mp\, v_0\,\frac{{\rm eV}^2}{\Delta m^2}\,L\left(\frac{T_\nu}{\rm MeV}\right)^4 y\,, \tag{12}$$

where the $-$ $(+)$ sign holds for neutrinos (antineutrinos) and $v_0 = (4\sqrt{2}\zeta(3)/\pi^2)10^{12}\,G_{\rm F}{\rm MeV}^2 \simeq 8$. If we assume that $|L_{\rm i}| \gg L_\star \simeq 0.4\times10^{-6}(y\,\Delta m^2/{\rm eV}^2)^{1/3}$, then the resonance condition is satisfied for $v_2(y,T_\nu,L)=1$. This implies that for positive $L_{\rm i}$ and positive $\Delta m^2$ there is a resonance only for antineutrinos at a resonant temperature

$$T_\nu^{\rm res}(y, L \gg L_\star) = \left(\frac{1}{v_0\,L\,y}\,\frac{\Delta m^2}{{\rm eV}^2}\right)^{\frac14}{\rm MeV} < T_\nu^{\rm res}(y,0)\,. \tag{13}$$

Notice that this resonance occurs at different times for different values of $y = y_{\rm res}$. The asymmetry grows with time from the initial value and $y_{\rm res}$ spans all neutrino distribution starting from a small value $y_{\rm res} \ll 1$ to large values $y_{\rm res} \gg 1$, as discussed in detail in Ref. [20]. Since this process occurs, in general, during electron-positron annihilations, the neutrino temperature gets smaller than the photon temperature and, making use of entropy conservation, one has

$$T_\nu = T\left[\frac{g_S(m_e/T)}{g_S(0)}\right]^{\frac13}\,, \tag{14}$$

where $g_S$ is the number of entropy density ultrarelativistic degrees of freedom. For $T_\nu^{\rm res}(y_{\rm res} \ll 1, L_{\rm i}) \lesssim 1\,{\rm MeV}$, neutrino collisions can be neglected and at the resonance one has antineutrino conversions into dark neutrinos starting from small $y_{\rm res} \ll 1$. If the resonance is crossed adiabatically, then all lightest antineutrinos are converted into dark neutrinos. Notice that if $L_{\rm i} < 0$, then simply lightest neutrinos are converted into dark neutrinos instead of antineutrinos. For definiteness, we will usually refer to the case $L_{\rm i} > 0$ in the following. More generally, to account also for non-adiabatic conversions, the fraction of converted neutrinos can be calculated using the Landau-Zener approximation:

$$f_{\nu_\mu\to\nu_{\rm dark}} \simeq 1 - e^{-\frac{\pi}{2}\,\gamma_{\rm res}}\,. \tag{15}$$

In this expression $\gamma_{\rm res}$ is the adiabaticity parameter at the resonance, given by

$$\gamma_{\rm res} = \frac{|\Delta m^2|\,\sin^2 2\theta_0}{2y\,T_\nu^{\rm res}\,H_{\rm res}}\,, \tag{16}$$

where $H_{\rm res} \simeq 0.2{\rm s}^{-1}\sqrt{g_\rho(T_{\rm res})}(T_{\rm res}/{\rm MeV})^2$ is the expansion rate at the resonance and $g_\rho$ is the number of energy density ultrarelativistic degrees of freedom. The Landau-Zener approximation has been shown to reproduce quite well the numerical results obtained solving density matrix equation [20]. For simplicity, we can make use of a monochromatic approximation equivalent to say that all neutrinos are converted instantaneously at $T_\nu^{\rm res}$ corresponding at $y_{\rm res} = 3.15$. Using the prescription in Ref. [20], in this case one has to use $\langle L\rangle \simeq L_{\rm f}/2 \simeq 0.2$ in the evaluation of the adiabaticity parameter, obtaining:

$$\gamma_{\rm res} \simeq 1.4\,\times 10^9\sqrt{\frac{10.75}{g_\rho(T_\nu^{\rm res})}}\left(\frac{\Delta m^2}{{\rm eV}^2}\right)^{\frac14}\sin^2 2\theta_0\,. \tag{17}$$

We will comment in the final remarks on the validity of the monochromatic approximation.

**Dark neutrino decays into dark photons mixed with photons**. In order to explain the ERB, we assume that the dark neutrinos produced by active-to-dark neutrino conversions in the presence of a pre-existing asymmetry decay into dark fermions $\psi'$ with mass $m_{\psi'}$ and into a superposition of a dark and standard photon that we denote by $\gamma'$. The probability that $\gamma'$ is detected as a photon, that can also be regarded as the decay branching ration into photons, is denoted by $\varepsilon$. The dark photon is kinematically mixed with the standard photon but the kinetic mixing will not play any role, as we will comment. The dark fermion is assumed to be quasi-degenerate with $\nu_0$, while we assume the dark photon mass $m_{\gamma'} \lesssim 10^{-15}\,{\rm eV}$ in order to evade the cosmological constraints from COBE/FIRAS for any value of the kinetic mixing parameter $\chi_0$ [22–25].[26]. We also assume that the decays can be described as fully non-relativistically so that, at the decay, $\gamma'$ has an energy

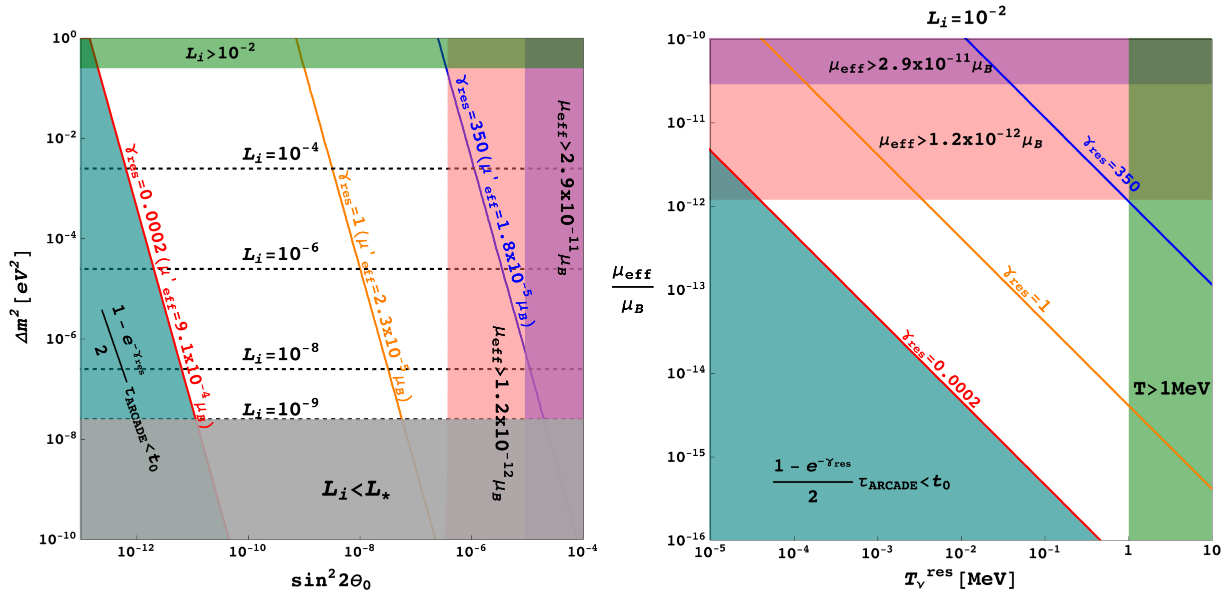


FIG. 3. Left panel: Constraints (shaded) and allowed region (white) in the plane of $\Delta m^2$ versus $\sin^2 2\theta_0$. The horizontal dashed lines give an upper bound on $\Delta m^2$ from $T_\nu^{\rm res} < 1\,\mathrm{MeV}$ for the indicated values of $L_{\rm i}$. Right panel: Constraints (shaded) and allowed region (white) in the plane of $\mu_{\rm eff}$ versus $T_\nu^{\rm res}$. We have used conservatively $\varepsilon = 1$.

$E_{\gamma'} \simeq \Delta m' \equiv m_0 - m_{\psi'}$. In this way the spectrum of non-thermal photons produced by the decays of the dark neutrinos and detected at the present time would be described by an effective temperature given exactly by the expression in Eq. (1) multiplied by $\varepsilon$ and also divided by a factor $2/(1-e^{-\frac{\pi}{2}\gamma_{\rm res}})$, taking into account that only relic antineutrinos are, adiabatically or non-adiabatically, converted into dark neutrinos.

The dark fermion radiative decay rate into $\gamma'$ can be related to a dark neutrino effective magnetic moment $\mu'_{\rm eff}$ by an expression analogous to Eq. (3):

$$\Gamma_{\nu_0\to\psi'+\gamma'} = \frac{(m_0^2 - m_{\psi'}^2)^3}{8\pi\, m_0^3}\,\mu'^2_{\rm eff} \simeq \frac{\Delta m'^3}{\pi}\,\mu'^2_{\rm eff} \simeq 42.5\,\mathrm{s}^{-1}\left(\frac{\Delta m'}{\mathrm{eV}}\right)^3\left(\frac{\mu'_{\rm eff}}{\mu_{\rm B}}\right)^2 . \quad (18)$$

The important difference is that now $\mu'_{\rm eff}$ does not have direct experimental constraints. However, because of the active-dark neutrino mixing, the active neutrino still has an effective neutrino magnetic moment $\mu_{\rm eff} = \sqrt{\varepsilon}\sin^2\theta_0\mu'_{\rm eff}$ and for this reason the experimental constraints on $\mu_{\rm eff}$ still play a role.

**Constraints and allowed region**. Let us now combine all constraints and determine the allowed region in the parameter space of interest. First, we determine a convenient minimum set of parameters to display all the constraints. We start by imposing that the non-thermal photons produced by the dark neutrino decays, and mixed with the dark photons, can reproduce the ARCADE 2 data. We have then to impose that the dark neutrino lifetime is given by the lifetime determined in [7] in the case of direct relic neutrino decays (see best fit in Fig. 1), that we denote by $\tau_{\rm ARCADE}(\nu_1 \to \nu_0 + \gamma)$, shortened by a factor $\varepsilon\,(1 - e^{-\gamma_{\rm res}})/2$ to compensate the reduced photon production, explicitly:

$$\tau_{\nu_0\to\psi'+\gamma'} = \frac{\varepsilon\,(1 - e^{-\gamma_{\rm res}})}{2}\tau_{\rm ARCADE}(\nu_1 \to \nu_0 + \gamma) \gtrsim t_0 \,. \quad (19)$$

On the other hand, the lifetime cannot be shorter than $t_0$, as also indicated in (19), since otherwise the exponential in the decay-law kicks in and suppresses the photon effective temperature below the ARCADE 2 measured values. Since the lifetime is the inverse of the decay rate given in Eq. (3), the constraint (19) allows to express $\mu'_{\rm eff}$ in terms of $\gamma_{\rm res}$. Therefore, for a fixed value of $\gamma_{\rm res}$, one has a fixed value of $\mu'_{\rm eff}$. At the same time $\gamma_{\rm res}$ is expressed in terms of $\sin^2 2\theta_0$ and $\Delta m^2$ from Eq. (17).

We also have to impose the constraint $T_\nu^{\rm res}(L_{\rm i}) \lesssim 1\,\mathrm{MeV}$, corresponding to a neutrino collisionless regime. From Eq. (13) one can see that, for a fixed value of $L_{\rm i}$, this results in an upper bound on $\Delta m^2$. Higher values of $L_{\rm i}$ correspond to higher allowed values of $\Delta m^2$. However, one has to impose an upper bound $L_{\rm i} \lesssim 10^{-2}$ from cosmological observations, since this would affect both BBN and CMB anisotropies [27]. It is then possible to express all other parameters in terms of $\sin^2 2\theta_0$, $\Delta m^2$ and $L_{\rm i}$. Therefore, we can conveniently show all constraints in the plane $\Delta m^2$ versus $\sin^2 2\theta_0$, as shown in the left panel of Fig. 3 for the most conservative choice $\varepsilon = 1$, corresponding to $\gamma' = \gamma$, and highest value of $\tau_{\rm ARCADE}(\nu_1 \to \nu_0 + \gamma)$ allowed at 99% C.L. (from Eq. (2)).

All constraints (shaded regions) are explicitly indicated. The horizontal dashed lines give the upper bound on $\Delta m^2$ for different values of $L_{\rm i}$. One can also notice the experimental constraints on $\mu_{\rm eff}$ that basically translate into an upper bound on $\sin^2 2\theta_0$. The orange line is the iso-contour line for $\gamma_{\rm res} = 1$, marking the border between the adiabatic and the non-adiabatic regime. In the right panel of Fig. 3 we also show constraints and allowed region in the plane $\mu_{\rm eff}$ versus $T_\nu^{\rm res}$ for the maximum allowed value of $L_{\rm i} = 10^{-2}$. As one can see, we find a very interesting lower bound $\mu_{\rm eff}/\mu_{\rm B} \gtrsim 10^{-16}$ which might be testable [28]. Taking smaller values of $L_{\rm i}$ moves up this lower bound on $\mu_{\rm eff}$, making it even easier to be tested.

**Final remarks**. (i) The boomerang mechanism effectively realizes a solution of the ERB mystery obtained in terms of radiative relic neutrino decays [7] but in two stages: in a first early stage relic antineutrinos (or neutrinos, depending on the sign of $L_{\rm i}$) of one species are converted into dark neutrinos (the visible sector throws particles into the dark sector); in a second stage dark neutrinos decay into dark-standard photon states (dark sector throws back particles into the visible one). (ii) As Fig. 3 shows, it has a broad variety of phenomenological implications that make it testable in different ways. First of all the TMS experiment will soon verify the ARCADE 2 data, the existence of the ERB and the solution proposed in Ref. [7]. Notice also that this implies some non-standard deviation in the 21 cm cosmological global signal (see [7] for details). Possible cosmological anomalies in BBN and/or CMB anisotropies might be addressed by the presence of a large lepton asymmetry [29]. Also notice that it implies non-standard relic neutrino background properties that might be potentially measured [20]. Finally, the lower bound we found on $\mu_{\rm eff}$, four orders of magnitude below the current upper bound, will be tested by future experiments [28]. (iii) The initial lepton asymmetry $L_{\rm i}$ can either be generated by some external mechanism, such as the decays of weekly coupled seesaw neutrinos as in leptogenesis [30], or, even more intriguingly, it could be generated dynamically by the same active-dark neutrino mixing [19, 20]. In this case, for $L_{\rm i} = 0$, the initial resonance at $T_\nu^{\rm res}(0) \gtrsim 1\,{\rm MeV}$ occurs in the collisional regime and triggers an initial exponential growth of the asymmetry. This stage would then provide the value we denoted by $L_{\rm i}$ needed for the conversion of active to dark neutrinos. This option might imply a reduced allowed region in the plane $\Delta m^2$ versus $\sin^2 2\theta_0$. (iv) The monochromatic approximation we used is well justified by numerical solution of density matrix equation with a full momentum description [20]. This also grasps the variation of the non-adiabaticity parameter with momentum. However, one would have small corrections to the allowed region we have derived. (v) The allowed regions have been determined for the most conservative case $\varepsilon = 1$, corresponding to the extreme minimal case where existence of dark photons would be not necessary. They would clearly shrink for lower values until they would disappear for a lower bound $\varepsilon \sim 2 \times 10^{-4}$. (vi) Having imposed $m_{\gamma'} < 10^{-15}\,{\rm eV}$ suppresses the kinetic mixing since $m_\gamma^2 \gg m_{\gamma'}^2$, evading microwave background constraints [22]. Since kinetic mixing is suppressed, we cannot have $\gamma' = \gamma_{\rm dark}$ (i.e., $\varepsilon = 0$) and a dynamical generation of a photon component due to a large kinetic mixing parameter $\chi_0$; also, since kinetic mixing does not play a role, one could optionally have $m_{\gamma'} > 10^{-15}\,{\rm eV}$ and negligible kinetic mixing without violating microwave background constraints. (vii) Notice that having $\varepsilon$ and $\theta_0 \neq 0$ could induce a non-vanishing neutrino millicharge in addition to an effective magnetic moment and this might introduce further constraints to be taken into account [11]. However, these constraints are model dependent and we have assumed that the neutrino millicharge is negligible. In any case these could be circumvented replacing a constant $\theta_0$ with a temperature dependent effective mixing angle such that $\theta(T_{\rm res}^\nu)$ coincides with the required values for the mechanism to work shown in the left panel of Fig. 3, while for $T \ll T_{\rm res}^\nu$ this is sufficiently small to generate a neutrino millicharge in agreement with all constraints. (viii) We also have to take into account stellar cooling constraints from plasmon decays $\gamma^\star \to \nu_0 + \psi'$. However, these can be circumvented coupling the dark fermions to a scalar in a way that either they get a mass higher than plasmon mass [31] or that the coupling to photons in stars is suppressed by having a symmetry restoration at an energy scale $\mathcal{O}({\rm keV})$ such that the scalar vev vanishes [32]. Interestingly, such a low scale phase transition has been proposed with independent motivations, within a split-seesaw Majoron model [33]. (ix) We have not discussed how the boomerang mechanism could be embedded within a full model. For example, a possible direction is offered by models incorporating quasi-Dirac neutrinos [34, 35]. Typically, we have maximal mixing for $\Delta m \ll m$, as $\tan 2\theta \sim 2m/\Delta m$, but arbitrary mixing is possible for certain textures of the Dirac and Majorana mass matrices, akin to the case of low-scale type-I seesaw [36]. Also notice that only within a definite model one could have more specific relation between $\varepsilon$ and $\chi_0$ and calculate neutrino millicharge and consequent contraints.

In conclusion, the boomerang mechanism shows that a solution to the ERB in terms of relic radiative neutrino decays is possible. If the excess will be confirmed, this might provide a direct open window to explore a new dark sector.

**Acknowledgments.** We thank Jens Chluba, André de Gouvêa, Chee Sheng Fong, Josè Alberto Rubiño Martin, Georg Raffelt, Pasquale Serpico, Alexander Studenikin and Anil Thapa for useful discussions. The work of BD was partly supported by the U.S. Department of Energy under grant No. DE-SC0017987. PDB and RR acknowledge financial support from the STFC Consolidated Grant ST/T000775/1. IMS is supported by STFC grant ST/T001011/1.

## End Matter

**Boomerang mechanism versus neutrino oscillation constraints.** Having obtained an allowed region in the $\Delta m^2$ versus $\sin^2 2\theta_0$ plane, we compare it with the existing constraints from neutrino oscillation experiments. Active research is underway on sterile neutrinos with masses around the eV scale, motivated by the excess observed by LSND [37], and the intriguing results reported by MiniBooNE [38], BEST [39], and IceCube [40]. However, many other experiments have not found such evidence, leading to significant tension among data sets when combined [41, 42].

Beyond the eV-scale sterile neutrino, searches have explored a wide range of mass for oscillations between active and sterile states [35, 43–53], but no evidence has been found. For nearly degenerate active and sterile states, solar [48, 54, 55], and reactor data [56], constrain $\Delta m^2 \lesssim 10^{-12}\text{eV}^2$ and $\sin^2 2\theta \lesssim 10^{-4}$, as shown in Fig. 4. The disappearance bounds of muons come from long-baseline experiments [57, 58] and atmospheric experiments [59], $\Delta m^2 \lesssim 10^{-4}$ eV$^2$ and $\sin^2 2\theta_0 \lesssim 10^{-2}$. Astrophysical neutrinos, with large $L/E$, probe down to $\Delta m^2 \sim 10^{-20}\text{eV}^2$ for maximal mixing [52, 60–64].

Fig. 4 compares current bounds with the region predicted by the boomerang mechanism (cf. Fig. 3 left panel). While this work focuses on muon-sterile oscillations, the mechanism applies to all flavors, so we used the strongest bounds over the mixing. Upcoming experiments like DARWIN [61] and JUNO [65] will further improve sensitivity.

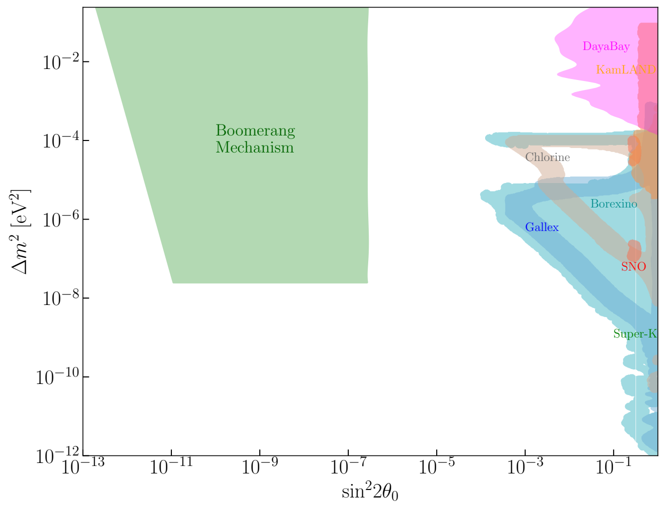


FIG. 4. Region allowed by the boomerang mechanism at 99% C.L., along with the region excluded by oscillation experiments. We present some of the most stringent bounds on the mixing, including measurements from solar neutrino experiments such as Borexino [55], Gallex [66], Chlorine [67], and SNO [68], Super-Kamiokande [69] as well as reactor experiments like KamLAND [55] and Daya Bay [56].

* bdev@wustl.edu
† P.Di-Bari@soton.ac.uk
‡ ivan.j.martinez-soler@durham.ac.uk
§ roshan@soton.ac.uk

[1] D. J. Fixsen *et al.*, ARCADE 2 Measurement of the Extra-Galactic Sky Temperature at 3-90 GHz, Astrophys. J. **734**, 5 (2011), arXiv:0901.0555 [astro-ph.CO].

[2] J. Singal *et al.*, The Radio Synchrotron Background: Conference Summary and Report, Publ. Astron. Soc. Pac. **130**, 036001 (2018), arXiv:1711.09979 [astro-ph.HE].

[3] G. P. Holder, The unusual smoothness of the extragalactic unresolved radio background, Astrophys. J. **780**, 112 (2014), arXiv:1207.0856 [astro-ph.CO].

[4] J. A. Rubiño Martín *et al.*, The Tenerife Microwave Spectrometer (TMS) experiment: studying the absolute spectrum of the sky emission in the 10-20GHz range, in *Millimeter, Submillimeter, and Far-Infrared Detectors and Instrumentation for Astronomy X*, Society of Photo-Optical Instrumentation Engineers (SPIE) Conference Series, Vol. 11453, edited by J. Zmuidzinas and J.-R. Gao (2020) p. 114530T.

[5] P. Alonso-Arias, P. A. Fuerte-Rodríguez, R. J. Hoyland, and J. A. Rubiño-Martín, The optical system of the Tenerife Microwave Spectrometer: a window for observing the 10–20 GHz sky spectra, JINST **16** (12), P12037, arXiv:2111.15364 [astro-ph.IM].

[6] M. Chianese, P. Di Bari, K. Farrag, and R. Samanta, Probing relic neutrino radiative decays with 21 cm cosmology, Phys. Lett. B **790**, 64 (2019), arXiv:1805.11717 [hep-ph].

[7] P. S. B. Dev, P. Di Bari, I. Martínez-Soler, and R. Roshan, Relic neutrino decay solution to the excess radio background, JCAP **04**, 046, arXiv:2312.03082 [hep-ph].

[8] D. J. Fixsen, The Temperature of the Cosmic Microwave Background, Astrophys. J. **707**, 916 (2009), arXiv:0911.1955 [astro-ph.CO].

[9] J. Dowell and G. B. Taylor, The Radio Background Below 100 MHz, Astrophys. J. Lett. **858**, L9 (2018), arXiv:1804.08581 [astro-ph.CO].

[10] Z.-z. Xing and S. Zhou, *Neutrinos in particle physics, astronomy and cosmology* (2011).

[11] C. Giunti and A. Studenikin, Neutrino electromagnetic interactions: a window to new physics, Rev. Mod. Phys. **87**, 531 (2015), arXiv:1403.6344 [hep-ph].

[12] G. G. Raffelt, New bound on neutrino dipole moments from globular cluster stars, Phys. Rev. Lett. **64**, 2856 (1990).

[13] F. Capozzi and G. Raffelt, Axion and neutrino bounds improved with new calibrations of the tip of the red-giant branch using geometric distance determinations, Phys. Rev. D **102**, 083007 (2020), arXiv:2007.03694 [astro-ph.SR].

[14] A. G. Beda, V. B. Brudanin, V. G. Egorov, D. V.

Medvedev, V. S. Pogosov, M. V. Shirchenko, and A. S. Starostin, Upper limit on the neutrino magnetic moment from three years of data from the GEMMA spectrometer, (2010), arXiv:1005.2736 [hep-ex].

[15] A. G. Beda, V. B. Brudanin, V. G. Egorov, D. V. Medvedev, V. S. Pogosov, M. V. Shirchenko, and A. S. Starostin, The results of search for the neutrino magnetic moment in GEMMA experiment, Adv. High Energy Phys. **2012**, 350150 (2012).

[16] The name 'boomerang' mechanism is justified by the fact that the visible sector first throws sterile neutrinos into the dark sector via mixing, and then these, decaying, throw back photons into the visible sector. The net result is that neutrinos are converted into photons. Trading off the effective magnetic moment of ordinary neutrinos with that of sterile neutrino to circumvent (5) is an ingredient, the only one, in common with the model proposed in Ref. [70] to explain the EDGES anomaly.

[17] We adopt a different sign convention for $\Delta m^2$ than in [20, 21].

[18] D. Nötzold and G. Raffelt, Neutrino dispersion at finite temperature and density, Nucl. Phys. B **307**, 924 (1988).

[19] R. Foot, M. J. Thomson, and R. R. Volkas, Large neutrino asymmetries from neutrino oscillations, Phys. Rev. D **53**, R5349 (1996), arXiv:hep-ph/9509327.

[20] P. Di Bari and R. Foot, Active sterile neutrino oscillations in the early universe: Asymmetry generation at low $|\delta m^2|$ and the Landau-Zener approximation, Phys. Rev. D **65**, 045003 (2002), arXiv:hep-ph/0103192.

[21] K. Enqvist, K. Kainulainen, and J. Maalampi, Refraction and Oscillations of Neutrinos in the Early Universe, Nucl. Phys. B **349**, 754 (1991).

[22] A. Mirizzi, J. Redondo, and G. Sigl, Microwave Background Constraints on Mixing of Photons with Hidden Photons, JCAP **03**, 026, arXiv:0901.0014 [hep-ph].

[23] A. Caputo, H. Liu, S. Mishra-Sharma, and J. T. Ruderman, Dark Photon Oscillations in Our Inhomogeneous Universe, Phys. Rev. Lett. **125**, 221303 (2020), arXiv:2002.05165 [astro-ph.CO].

[24] A. A. Garcia, K. Bondarenko, S. Ploeckinger, J. Pradler, and A. Sokolenko, Effective photon mass and (dark) photon conversion in the inhomogeneous Universe, JCAP **10**, 011, arXiv:2003.10465 [astro-ph.CO].

[25] G. Arsenadze, A. Caputo, X. Gan, H. Liu, and J. T. Ruderman, Shaping dark photon spectral distortions, JHEP **03**, 018, arXiv:2409.12940 [astro-ph.CO].

[26] Here we do not assume the dark photon to be dark matter in which case the bounds on $m_{\gamma'}$ would be more stringent [71]. Moreover, we do not consider the Juno constraint on $m_{\gamma'}$ that extends down to $m_{\gamma'} \sim 10^{-18}$ eV [72], as we lack a detailed understanding of the Jovian magnetosphere and the associated uncertainties.

[27] A. D. Dolgov, S. H. Hansen, S. Pastor, S. T. Petcov, G. G. Raffelt, and D. V. Semikoz, Cosmological bounds on neutrino degeneracy improved by flavor oscillations, Nucl. Phys. B **632**, 363 (2002), arXiv:hep-ph/0201287.

[28] C. Giunti, K. Kouzakov, Y.-F. Li, and A. Studenikin, Neutrino Electromagnetic Properties 10.1146/annurev-nucl-102122-023242 (2024), arXiv:2411.03122 [hep-ph].

[29] A.-K. Burns, T. M. P. Tait, and M. Valli, Indications for a Nonzero Lepton Asymmetry from Extremely Metal-Poor Galaxies, Phys. Rev. Lett. **130**, 131001 (2023), arXiv:2206.00693 [hep-ph].

[30] M. Fukugita and T. Yanagida, Baryogenesis Without Grand Unification, Phys. Lett. B **174**, 45 (1986).

[31] W. DeRocco, P. W. Graham, and S. Rajendran, Exploring the robustness of stellar cooling constraints on light particles, Phys. Rev. D **102**, 075015 (2020), arXiv:2006.15112 [hep-ph].

[32] R. N. Mohapatra and S. Nasri, Reconciling the CAST and PVLAS results, Phys. Rev. Lett. **98**, 050402 (2007), arXiv:hep-ph/0610068.

[33] P. Di Bari and M. H. Rahat, Split Majoron model confronts the NANOGrav signal and cosmological tensions, Phys. Rev. D **110**, 055019 (2024), arXiv:2307.03184 [hep-ph].

[34] K. S. Babu, X.-G. He, M. Su, and A. Thapa, Naturally light Dirac and pseudo-Dirac neutrinos from left-right symmetry, JHEP **08**, 140, arXiv:2205.09127 [hep-ph].

[35] K. Carloni, I. Martínez-Soler, C. A. Arguelles, K. S. Babu, and P. S. B. Dev, Probing pseudo-Dirac neutrinos with astrophysical sources at IceCube, Phys. Rev. D **109**, L051702 (2024), arXiv:2212.00737 [astro-ph.HE].

[36] J. Kersten and A. Y. Smirnov, Right-Handed Neutrinos at CERN LHC and the Mechanism of Neutrino Mass Generation, Phys. Rev. D **76**, 073005 (2007), arXiv:0705.3221 [hep-ph].

[37] A. Aguilar *et al.* (LSND), Evidence for neutrino oscillations from the observation of $\bar{\nu}_e$ appearance in a $\bar{\nu}_\mu$ beam, Phys. Rev. D **64**, 112007 (2001), arXiv:hep-ex/0104049.

[38] A. A. Aguilar-Arevalo *et al.* (MiniBooNE), Updated MiniBooNE neutrino oscillation results with increased data and new background studies, Phys. Rev. D **103**, 052002 (2021), arXiv:2006.16883 [hep-ex].

[39] V. V. Barinov *et al.*, Results from the Baksan Experiment on Sterile Transitions (BEST), Phys. Rev. Lett. **128**, 232501 (2022), arXiv:2109.11482 [nucl-ex].

[40] R. Abbasi *et al.* ((IceCube Collaboration)‖, IceCube), Search for an eV-Scale Sterile Neutrino Using Improved High-Energy $\nu\mu$ Event Reconstruction in IceCube, Phys. Rev. Lett. **133**, 201804 (2024), arXiv:2405.08070 [hep-ex].

[41] M. Dentler, Á. Hernández-Cabezudo, J. Kopp, P. A. N. Machado, M. Maltoni, I. Martinez-Soler, and T. Schwetz, Updated Global Analysis of Neutrino Oscillations in the Presence of eV-Scale Sterile Neutrinos, JHEP **08**, 010, arXiv:1803.10661 [hep-ph].

[42] J. M. Hardin, I. Martinez-Soler, A. Diaz, M. Jin, N. W. Kamp, C. A. Argüelles, J. M. Conrad, and M. H. Shaevitz, New Clues about light sterile neutrinos: preference for models with damping effects in global fits, JHEP **09**, 058, arXiv:2211.02610 [hep-ph].

[43] L. Wolfenstein, Different Varieties of Massive Dirac Neutrinos, Nucl. Phys. B **186**, 147 (1981).

[44] S. T. Petcov, On Pseudodirac Neutrinos, Neutrino Oscillations and Neutrinoless Double beta Decay, Phys. Lett. B **110**, 245 (1982).

[45] S. M. Bilenky and B. Pontecorvo, Neutrino Oscillations With Large Oscillation Length in Spite of Large (Majorana) Neutrino Masses?, Sov. J. Nucl. Phys. **38**, 248 (1983).

[46] M. Kobayashi and C. S. Lim, Pseudo Dirac scenario for neutrino oscillations, Phys. Rev. D **64**, 013003 (2001), arXiv:hep-ph/0012266.

[47] G. Anamiati, R. M. Fonseca, and M. Hirsch, Quasi Dirac neutrino oscillations, Phys. Rev. D **97**, 095008 (2018), arXiv:1710.06249 [hep-ph].

[48] A. de Gouvea, W.-C. Huang, and J. Jenkins, Pseudo-Dirac Neutrinos in the New Standard Model, Phys. Rev. D **80**, 073007 (2009), arXiv:0906.1611 [hep-ph].

[49] F. Vissani and A. Boeltzig, Supernova Neutrinos: Risks and Opportunities, PoS **NEUTEL2015**, 008 (2015).

[50] I. M. Shoemaker and K. Murase, Probing BSM Neutrino Physics with Flavor and Spectral Distortions: Prospects for Future High-Energy Neutrino Telescopes, Phys. Rev. D **93**, 085004 (2016), arXiv:1512.07228 [astro-ph.HE].

[51] V. Brdar and R. S. L. Hansen, IceCube Flavor Ratios with Identified Astrophysical Sources: Towards Improving New Physics Testability, JCAP **02**, 023, arXiv:1812.05541 [hep-ph].

[52] A. De Gouvêa, I. Martinez-Soler, Y. F. Perez-Gonzalez, and M. Sen, Fundamental physics with the diffuse supernova background neutrinos, Phys. Rev. D **102**, 123012 (2020), arXiv:2007.13748 [hep-ph].

[53] T. Rink and M. Sen, Constraints on pseudo-Dirac neutrinos using high-energy neutrinos from NGC 1068, Phys. Lett. B **851**, 138558 (2024), arXiv:2211.16520 [hep-ph].

[54] S. Ansarifard and Y. Farzan, Revisiting pseudo-Dirac neutrino scenario after recent solar neutrino data, Phys. Rev. D **107**, 075029 (2023), arXiv:2211.09105 [hep-ph].

[55] Z. Chen, J. Liao, J. Ling, and B. Yue, Constraining super-light sterile neutrinos at Borexino and KamLAND, JHEP **09**, 004, arXiv:2205.07574 [hep-ph].

[56] F. P. An *et al.* (Daya Bay), Search for a Sub-eV Sterile Neutrino using Daya Bay's Full Dataset, Phys. Rev. Lett. **133**, 051801 (2024), arXiv:2404.01687 [hep-ex].

[57] P. Adamson *et al.* (MINOS+), Search for sterile neutrinos in MINOS and MINOS+ using a two-detector fit, Phys. Rev. Lett. **122**, 091803 (2019), arXiv:1710.06488 [hep-ex].

[58] M. A. Acero *et al.* (NOvA), Dual-Baseline Search for Active-to-Sterile Neutrino Oscillations in NOvA, Phys. Rev. Lett. **134**, 081804 (2025), arXiv:2409.04553 [hep-ex].

[59] J. F. Beacom, N. F. Bell, D. Hooper, J. G. Learned, S. Pakvasa, and T. J. Weiler, PseudoDirac neutrinos: A Challenge for neutrino telescopes, Phys. Rev. Lett. **92**, 011101 (2004), arXiv:hep-ph/0307151.

[60] I. Martinez-Soler, Y. F. Perez-Gonzalez, and M. Sen, Signs of pseudo-Dirac neutrinos in SN1987A data, Phys. Rev. D **105**, 095019 (2022), arXiv:2105.12736 [hep-ph].

[61] A. de Gouvêa, E. McGinness, I. Martinez-Soler, and Y. F. Perez-Gonzalez, pp solar neutrinos at DARWIN, Phys. Rev. D **106**, 096017 (2022), arXiv:2111.02421 [hep-ph].

[62] C. S. Fong and Y. Porto, Constraining pseudo-Diracness with astrophysical neutrino flavors, (2024), arXiv:2406.15566 [hep-ph].

[63] P. S. B. Dev, P. A. N. Machado, and I. Martinez-Soler, Pseudo-Dirac neutrinos and relic neutrino matter effect on the high-energy neutrino flavor composition, Phys. Lett. B **862**, 139306 (2025), arXiv:2406.18507 [hep-ph].

[64] K. Carloni, Y. Porto, C. A. Argüelles, P. S. B. Dev, and S. Jana, Signatures of quasi-Dirac neutrinos in diffuse high-energy astrophysical neutrino data, (2025), arXiv:2503.19960 [hep-ph].

[65] J. Franklin, Y. F. Perez-Gonzalez, and J. Turner, JUNO as a probe of the pseudo-Dirac nature using solar neutrinos, Phys. Rev. D **108**, 035010 (2023), arXiv:2304.05418 [hep-ph].

[66] W. Hampel *et al.* (GALLEX), GALLEX solar neutrino observations: Results for GALLEX IV, Phys. Lett. B **447**, 127 (1999).

[67] B. T. Cleveland, T. Daily, R. Davis, Jr., J. R. Distel, K. Lande, C. K. Lee, P. S. Wildenhain, and J. Ullman, Measurement of the solar electron neutrino flux with the Homestake chlorine detector, Astrophys. J. **496**, 505 (1998).

[68] Q. R. Ahmad *et al.* (SNO), Direct evidence for neutrino flavor transformation from neutral current interactions in the Sudbury Neutrino Observatory, Phys. Rev. Lett. **89**, 011301 (2002), arXiv:nucl-ex/0204008.

[69] S. Fukuda *et al.* (Super-Kamiokande), Solar B-8 and hep neutrino measurements from 1258 days of Super-Kamiokande data, Phys. Rev. Lett. **86**, 5651 (2001), arXiv:hep-ex/0103032.

[70] D. Aristizabal Sierra and C. S. Fong, The EDGES signal: An imprint from the mirror world?, Phys. Lett. B **784**, 130 (2018), arXiv:1805.02685 [hep-ph].

[71] A. Caputo, A. J. Millar, C. A. J. O'Hare, and E. Vitagliano, Dark photon limits: A handbook, Phys. Rev. D **104**, 095029 (2021), arXiv:2105.04565 [hep-ph].

[72] S. Yan, L. Li, and J. Fan, Constraints on photon mass and dark photon from the Jovian magnetic field, JHEP **06**, 028, arXiv:2312.06746 [hep-ph].